Engineering quantum-coherent defects: The role of substrate miscut in chemical vapor deposition diamond growth ©

Cite as: Appl. Phys. Lett. 117, 194001 (2020); https://doi.org/10.1063/5.0029715 Submitted: 15 September 2020 . Accepted: 22 October 2020 . Published Online: 13 November 2020

Simon A. Meynell, Claire A. McLellan, Lillian B. Hughes, Wenbo Wang, 🔟 Tom E. Mates, Kunal Mukherjee, and 🔟 Ania C. Bleszynski Jayich

COLLECTIONS

EP

This paper was selected as an Editor's Pick







ARTICLES YOU MAY BE INTERESTED IN

Laser stimulated THz emission from Pt/CoO/FeCoB

Applied Physics Letters 117, 192403 (2020); https://doi.org/10.1063/5.0020020

Periodic vortex-antivortex pairs in tensile strained PbTiO3 films

Applied Physics Letters 117, 192901 (2020); https://doi.org/10.1063/5.0023871

A highly sensitive, large area, and self-powered UV photodetector based on coalesced gallium nitride nanorods/graphene/silicon (111) heterostructure

Applied Physics Letters 117, 191103 (2020); https://doi.org/10.1063/5.0018076



Your Qubits. Measured.

Meet the next generation of quantum analyzers

- Readout for up to 64 qubits
- Operation at up to 8.5 GHz, mixer-calibration-free
- Signal optimization with minimal latency





Cite as: Appl. Phys. Lett. **117**, 194001 (2020); doi: 10.1063/5.0029715 Submitted: 15 September 2020 · Accepted: 22 October 2020 · Published Online: 13 November 2020







Simon A. Meynell,^{1,a)} Claire A. McLellan,² Lillian B. Hughes,³ Wenbo Wang,¹ Tom E. Mates,³ (ib) Kunal Mukherjee,³ and Ania C. Bleszynski Jayich¹ (ib)

AFFILIATIONS

- ¹Physics Department, University of California, Santa Barbara, Santa Barbara, California 93106, USA
- ²Department of Materials Science and Engineering, Stanford University, Stanford, California 94305, USA
- ³Materials Department, University of California, Santa Barbara, Santa Barbara, California 93117, USA

ABSTRACT

The engineering of defects in diamond, particularly nitrogen-vacancy (NV) centers, is important for many applications in quantum science. A materials science approach based on chemical vapor deposition (CVD) growth of diamond and *in situ* nitrogen doping is a promising path toward tuning and optimizing the desired properties of the embedded defects. Herein, with the coherence of the embedded defects in mind, we explore the effects of substrate miscut on the diamond growth rate, nitrogen density, and hillock defect density, and we report an optimal angle range for the purposes of engineering coherent ensembles of NV centers in diamond according to our growth parameters. We provide a model that quantitatively describes hillock nucleation in the step-flow regime of CVD growth, shedding insight on the physics of hillock formation. We also report significantly enhanced incorporation of nitrogen at hillock defects, opening the possibility for templating hillock-defect-localized NV center ensembles for quantum applications.

Published under license by AIP Publishing. https://doi.org/10.1063/5.0029715

Point defects in the solid state are a promising platform for quantum science and technology. 1-3 Diamond is a particularly attractive host material because of its high Debye temperature, wide bandgap, and deep level defects, allowing for the investigation of its defect qubits up to and above room temperature.4 Engineering the local environment of the qubits, both the bulk material and proximal surface, is crucial to their performance, affecting quantum coherence, 5-7 charge state,⁸ and indistinguishability of qubits.^{9,10} Furthermore, controlling the defect density and distribution while maintaining material quality is important; for example, dense and homogeneous defect layers are required for spin ensemble-based sensing and studies of quantum many-body spin dynamics, while coherent, near-surface defects allow for high spatial resolution imaging and coupling to other quantum elements such as phonons and photons. Surface quality and morphology are also important in maintaining high quality factors of the diamond photonic and phononic cavities utilized in spin-phonon¹¹ and spinphoton coupling schemes. 12-

Nitrogen-vacancy (NV) centers in diamond are presently the most widely studied diamond qubit, featuring a broad range of applications in quantum sensing, networks, and computing. Natural occurrence and ion implantation are two common ways to realize NV centers; however, in recent years, the *in situ* doping of nitrogen during plasma-enhanced chemical vapor deposition (CVD) diamond growth has become a key technique in the field. ^{16–18} Homoepitaxial CVD growth produces a high-quality crystalline lattice with high isotopic and chemical purity, thus creating a low magnetic noise environment for preserving qubit coherence. Furthermore, the gentle, bottom-up incorporation of nitrogen into this matrix via *in situ* doping provides a means for both controlling the depth localization to the nanometer scale¹⁷ and reliably producing homogeneous, coherent NV ensembles.¹⁹ The technique of CVD growth is well understood,²⁰ and previous works have explored dopant incorporation into diamond films,^{21–25} but few studies consider defect density and localization with the requirements of quantum applications in mind.

Herein, we explore the CVD growth of nitrogen-doped (100) diamond films as it uniquely relates to quantum applications involving quantum defects. Working in the slow ($<10\,\text{nm/h}$) growth rate regime, we systematically investigate and quantify the growth rate,

a) Author to whom correspondence should be addressed: simonmeynell@physics.ucsb.edu

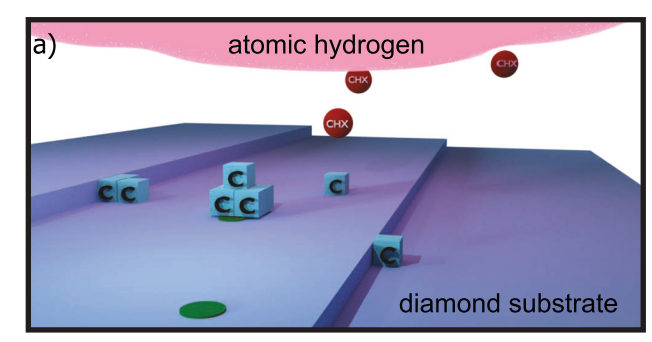
defect properties (density, coherence, and spatial distribution), and surface quality as a function of substrate miscut. We provide a model that quantitatively describes hillock nucleation in the step-flow regime of CVD growth, shedding insight on the physics of hillock formation. Altogether, we report an optimal miscut angle range between $0.7^{\circ} \lesssim \theta \lesssim 1.2^{\circ}$ for the purposes of engineering coherent ensembles of NV centers in diamond for quantum applications.

Substrate miscut plays an important role in diamond CVD growth, as the dominant growth mechanism is thought to occur via carbon adatom incorporation at step-edge sites, ^{20,26} as illustrated in the schematic of Fig. 1(a), and the miscut determines the density of step-edges on the surface. Furthermore, the formation of certain defects, particularly the laterally extended, flat types of growth called hillocks, occurs via a step-edge dependent mechanism. ^{27,28} These defects can both serve as a probe of the growth mode and an intriguing means of locally controlling defect density.

To systematically explore the influence of miscut, we utilize a single sample with five regions, each polished to a different miscut angle (RMS roughness <200 pm). ²⁹ By using a single sample, we avoid sample to sample variations in substrate and sample preparation. An optical image of this sample is shown in Fig. 1(b). The miscut angle was varied discretely in 0.5° steps across the sample, forming five different regions with miscut ranging from an absolute value of $|\theta| = 0.16^{\circ} - 1.66^{\circ}$. The incremental difference between regions was confirmed with atomic force microscopy [Fig. 1(c)] and the miscuts were verified by x-ray diffraction (XRD), using glancing incidence reflectivity measurements to align the beam relative to the surface normal and subsequently performing a rocking curve measurement about the (004) peak.

Homoepitaxial CVD diamond growth on the multi-angle-polished substrate proceeded in the process optimized in Ref. 17 using a SEKI AX6300 plasma enhanced chemical vapor deposition tool. Specifically, the growth consisted of a 3-h undoped diamond buffer layer using 0.1 sccm of 99.999% $^{12}\mathrm{C}$ enriched isotopically purified methane and 400 sccm of H₂ at 800 °C, chamber pressure of 25 Torr, and microwave power of 750 W. The buffer layer was followed by a 6-h nitrogen-doped growth using 5 sccm of 98% $^{15}\mathrm{N}$ enriched nitrogen and 0.1 sccm isotopically purified methane. In the last step, the sample was capped with a 4-h undoped layer using 0.1 sccm isotopically purified methane. After growth, the diamond was irradiated with 145 keV electrons (total fluence $\sim 10^{17}\,e^-/\mathrm{cm}^2$) to create vacancies and subsequently annealed to form NV centers. Annealing was performed in Ar/H gas at 800 °C for 8 h with a 16-h ramp time.

We first discuss the effect of substrate miscut on the growth rate of the diamond. Because the growth is performed with isotopically purified methane, the thickness of the grown layer, d_0 , can be determined by measuring the thickness of the 13 C-depleted layer via secondary ion mass spectrometry (SIMS). Figure 2(a) shows the 13 C depth profiles in each of the five miscut regions, offset by increasing factors of 10 for ease of readability. Each plot is averaged over several $\sim 100 \times 100 \, \mu \text{m}^2$ spots within each miscut region. Figure 2(b) shows the linear increase in d_0 with the miscut angle. This linearity suggests that the growth proceeds by a step-flow mechanism, which depends on the density of step edges on the surface. In this type of growth, the growth velocity, v_g , is related to the step velocity, v_s , and shallow miscut angle, θ , as $v_g = v_s \sin \theta \approx v_s \theta$. Thus, v_s can be obtained from the slope of Fig. 2(b), yielding $v_s \sim 100 \, \text{pm/s}$.



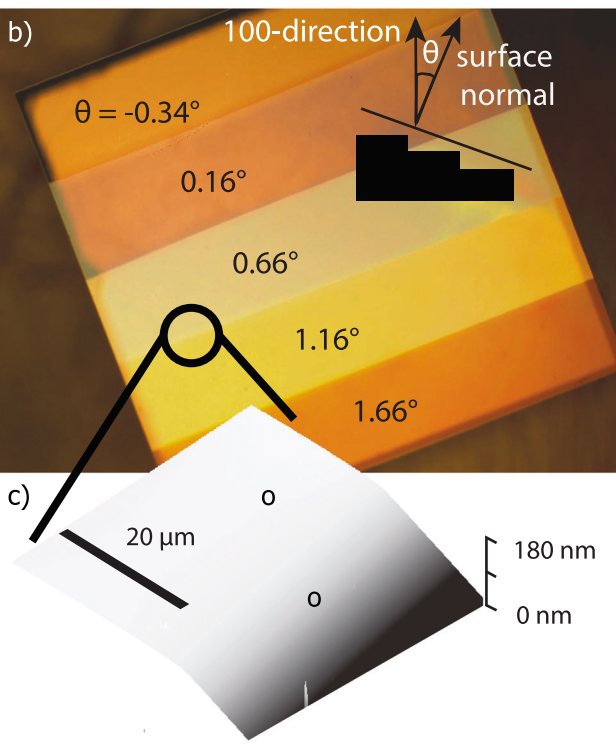


FIG. 1. (a) A schematic depiction of diamond growth. The steps shown in the image are the result of the substrate miscut and are crucially important for diamond growth. Carbon incorporates preferentially at the step edges and at defects illustrated by the green circles. (b) An optical image of the surface of the diamond substrate polished at five different miscuts, with the miscut angle specified on each slice. (c) An AFM image taken near the transition between two miscut regions shown in (b).

Because v_s appears constant over the range of miscut angles studied, it follows that the step velocity is independent of the angle, implying that the growth is dictated by the number density of available sites for carbon adatoms. The growth mode is thus a step-limited one, rather than the adatom-limited regime that is typical in molecular beam epitaxy (MBE) growth. We also note that for small θ , the growth rate does not go to zero $[d_0(\theta=0)=28\,\mathrm{nm}]$, indicating the dominance of a different growth mechanism in this regime. This non-zero growth rate for a zero-miscut surface could be explained by disordered step-flow resulting from entropically stabilized steps or the presence of

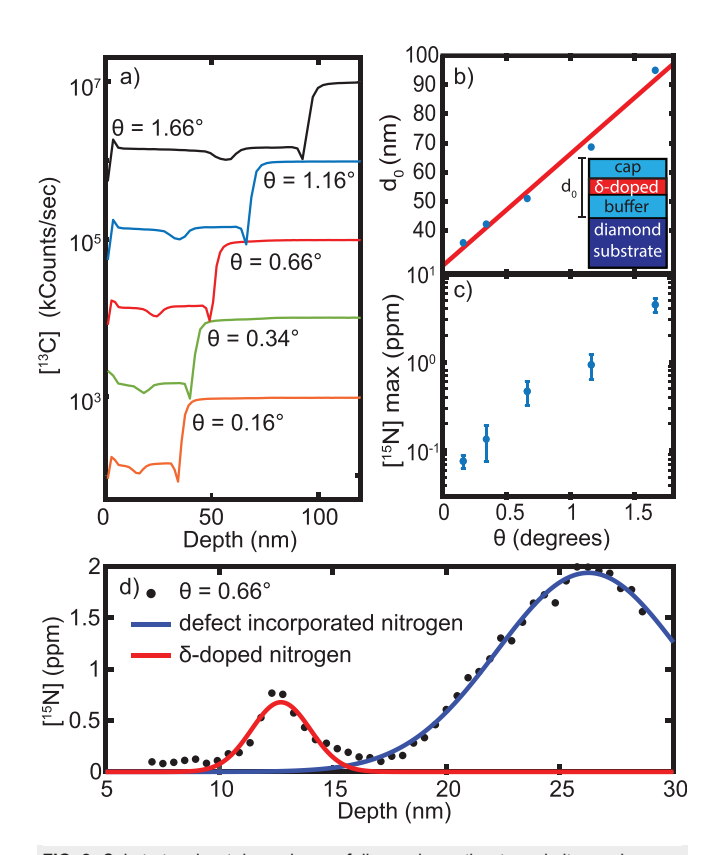


FIG. 2. Substrate miscut dependence of diamond growth rate and nitrogen incorporation in CVD-grown diamond. (a) $^{13}\mathrm{C}$ concentration as a function of depth as measured via SIMS for the five miscut angles studied. The depleted $^{13}\mathrm{C}$ layer indicates the grown diamond layer studied here. Profiles are offset by increasing factors of 10 for ease of readability, starting with $\theta=0.16^\circ$. (b) The thickness of the grown layer, d_0 , and (c) maximum concentration of the doped [$^{15}\mathrm{N}$] as a function of miscut. (d) A SIMS depth profile of $^{15}\mathrm{N}$ concentration in the $|\theta|=0.66^\circ$ miscut region. The two peaks correspond to $^{15}\mathrm{N}$ introduced via regular step-flow growth during in situ doping and $^{15}\mathrm{N}$ present in the hillocks, respectively. The maximum value of the smaller in situ-doped peak is plotted in (c). The SIMS dopant concentration is measured using a $^{12}\mathrm{C}^{15}\mathrm{N}$ complex and a relative sensitivity factor of 2.5×10^{20} atoms/cm³, which is corrected from the value given in Ref. 31 for the natural bulk carbon matrix. Even though the defect incorporated nitrogen and δ-doped nitrogen are introduced into the diamond at the same time, due to growth rate differences between the two growth-phases, the two nitrogen sources appear at different depths in our SIMS measurements.

another growth mode arising from defects. Finally, we attribute the dip in the [13 C] near $d/d_0=0$ to be an artifact of SIMS and the dip at $d/d_0=1$ to be the result of the growth reaching a steady state as the plasma is ignited. The dip occurring at $d/d_0\sim 0.5$ corresponds to the *in situ* nitrogen-doped layer and likely suggests that the introduction of nitrogen changes the plasma, resulting in an altered relative isotope abundance and growth rate.

The incorporation of nitrogen during growth is also found to depend strongly on the substrate miscut angle. Figure 2(c) plots the peak ^{15}N concentration in the *in situ*-doped layer measured via SIMS as a function of miscut. The SIMS dopant concentration is measured using a $^{12}C^{15}N$ complex and a relative sensitivity factor of 2.5×10^{20} atoms/cm³, which is corrected from the value given in Ref. 31 for the natural bulk carbon matrix. The ^{15}N dopant

concentration is found to be $\approx 0.1-10$ ppm consistent with the results of previous work under similar growth and doping parameters.¹⁷ The increase in nitrogen concentration with step-edge density is consistent with the findings of Ref. 33 and suggests that the nitrogen preferentially incorporates into steps. Examination of the SIMS ¹⁵N depth profiles in each region shows the presence of two distinct Gaussian peaks, with a representative example shown in Fig. 2(d). The first, smaller peak in the profile is found at the depth expected given the growth rate for that miscut region and the time of nitrogen introduction in the doped layer. It is the amplitude of this peak that is plotted in Fig. 2(c). The second, broad peak is attributed to nitrogen incorporation in non-step-flow related growth features, such as hillocks or unepitaxial crystallites. Whereas the small peak shows up at a consistent depth and amplitude across spots within the same miscut slice, the broad, defectrelated peak exhibits substantial variability from spot to spot within the same miscut slice (over an area of $\sim 100 \times 100 \, \mu \text{m}^2$). This variability is consistent with the observed variability of defect density across the sample. Further evidence for our interpretation of these two peaks is presented in the supplementary material.

We next extend our investigation of diamond growth through selective miscut to the formation of defects such as hillocks. Figures 3(a) and 3(b) show optical images of post-growth surfaces of the 0.16° and 0.66° regions. The dominant feature in both images is the presence of hillocks: square, flat-topped defects that are tens of nanometers tall. An atomic force microscopy (AFM) image of a hillock defect in diamond is shown in Fig. 3(d). A few of the hillocks also feature an additional unepitaxial crystallite²⁷ in their center, as shown in the scanning electron microscope (SEM) image in Fig. 3(e). The density of hillock defects is found to be inversely proportional to miscut, as seen qualitatively in the images of Figs. 3(a) and 3(b) and plotted quantitatively for all five angles in Fig. 3(c). For angles $\gtrsim 1.66^{\circ}$, however, the growth mode appears to transition into a step-bunching growth regime, similar to that reported in Refs. 34 and 35 and results in anisotropic defects as seen in Fig. 3(f). In order to preserve the well-behaved step-flow mode of growth, an optimal miscut angle less than $\sim 1.66^{\circ}$ is desirable.

In order to understand the mechanisms of hillock growth, we present a simple quantitative model of hillock nucleation and stabilization. For shallow angles, the miscut will be related to the step dimensions as $\theta=s/L$, where s is the step height and L is the step length as shown in the inset of Fig. 3(c). The hillocks attempt to form at sites with a density ρ_{H0} . Once a hillock begins nucleating, it will continue growing and will stabilize unless an incoming step suppresses it. The time required for the hillock to reach the point of stability is defined as T_{HD}^{28} and the probability of any given hillock successfully nucleating will be given by

$$P = 1 - \frac{v_s T_H}{L} = 1 - \frac{v_s T_H \theta}{s},$$
 (1)

and so the hillock density will be given by

$$\rho_H = \rho_{H0} \left(1 - \frac{v_s T_H \theta}{s} \right). \tag{2}$$

This model also predicts a critical angle, $\theta_C = s/v_s T_h$, at which the number of hillocks goes to zero, a result that is consistent with other observations of the hillock defect²¹ and implies that at θ_C the step length is not large enough to support a hillock before lateral

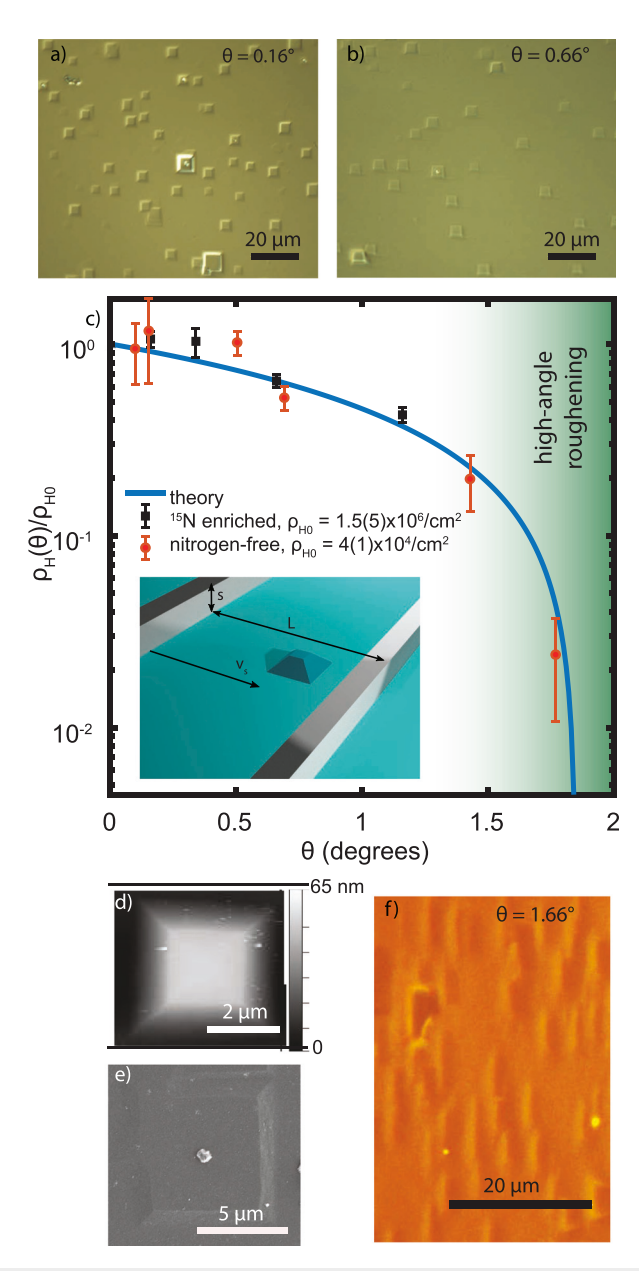


FIG. 3. Optical images of hillocks in the (a) $\theta=0.16^\circ$ and (b) $\theta=0.66^\circ$ regions on the multi-angle sample showing increased surface defect density at higher miscuts. (c) Hillock density (ρ_H) normalized by ρ_{H0} (hillock density at $\theta=0^\circ$) as a function of miscut angle for both nitrogen-doped and undoped diamond. Inset: schematic of the theoretical model for hillock formation and growth. At angles above \$\geq 1.66^\circ\$, step-bunching-type growth results in hillock suppression and surface roughening via enhanced lateral growth, as seen in (f), making quantitative assignment of hillock density difficult for the $\theta=1.66^\circ$ region of the doped diamond sample. (d) AFM and (e) SEM images of a hillock with and without an unepitaxial crystallite in its center. (f) Optical image of the $\theta=1.66^\circ$ region illustrating high-angle surface roughening.

growth of a step edge reaches it. Fitting data in Fig. 3(c), which also includes data for several independently grown, undoped nitrogen samples, we determine $\theta_C = 1.9 \pm 0.2^{\circ}$. Taking ν_s as determined before to be ~ 100 pm/s, the time for hillock formation is then given by

$$T_H = \frac{s}{\nu_s \theta_C} \approx 100 \,\mathrm{ms}.$$
 (3)

The value of ρ_{H0} is found by extracting the y-intercept of the fit in Fig. 3(c). The extracted value of ρ_{H0} differs dramatically for the doped nitrogen sample $[\rho_{H0}=1.5(0.5)\times 10^6~{\rm cm}^{-2}]$ and for the independently grown, undoped nitrogen samples [$\rho_{H0} = 4(1) \times 10^4 \text{ cm}^{-2}$]. The undoped nitrogen growths were performed on five independent substrates with similar growth parameters and epitaxial thicknesses of 80-120 nm. Despite the radical difference in nitrogen doping, the similarity in the two curves after normalization by ρ_{H0} indicates the broad applicability of the model. The two orders of magnitude difference between the hillock densities in doped and undoped samples suggests that nitrogen adatoms may be providing additional sites for hillock nucleation. Other doped nitrogen growths with similar doping parameters also exhibit commensurately high hillock densities. The hillock density of the undoped sample is roughly equal to the density of dislocations reported by Tokuda²⁸ and suggests that for undoped diamond growth, the primary source for hillock nucleation is preexisting dislocations, aligning with the findings of Ref. 27.

Interestingly, we find that the concentration of nitrogen is significantly enhanced at hillock sites, as shown in the spatially resolved SIMS and correlated optical images of Fig. 4. The spatial SIMS analysis is acquired across an $\sim\!100\times100\,\mu\text{m}^2$ area using a 1 nA Cs $^+$ ion beam with a spot size resolution of 2 μm , and the images are accumulated over a depth extent of $\sim\!4$ nm. ^{15}N counts within the hillocks are up to $\sim\!30$ larger compared to the bulk. To confirm that the observed ^{15}N enhancement is not a morphology-induced SIMS artifact, we also performed spatial analysis of the ^{12}C background and found no features in the images. These results further support our conclusion concerning the second, large peak observed in the ^{15}N SIMS depth profile of Fig. 2(d): ^{15}N incorporates inhomogeneously during CVD growth and shows preference for the step-edges of the hillock defects.

Finally, we probe the spin properties of the NV centers across the sample using scanning confocal microscopy and optically detected electron spin resonance (ESR). Figure 5 shows a confocal image and corresponding ESR spectra in the $\theta=0.66^\circ$ region: single, resolvable NV centers are observed across the sample and ensembles of NV centers are seen within hillocks and unepitaxial defects. The significantly higher NV photoluminescence signal from the defects is consistent with the expected higher NV density due to increased N incorporation. The linewidth of the ESR peaks in the 11 hillocks without unepitaxial defects measured is $\Gamma=2.9\pm0.2\,\mathrm{MHz}$, with a resolvable $^{15}\mathrm{N}$ hyperfine splitting. The unepitaxial defects, however, exhibit much

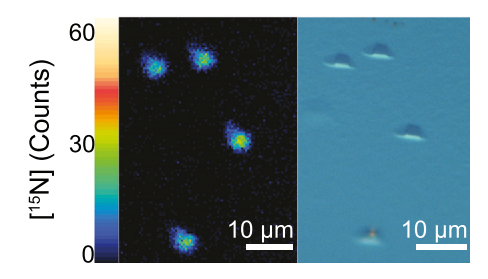


FIG. 4. Spatially resolved SIMS image (left) (Cs $^+$ ion beam, 1 nA, 15 keV, 2 μ m spot size, 6000 M/ Δ M) showing 15 N enrichment at hillocks and corresponding optical image of the targeted hillocks (right).

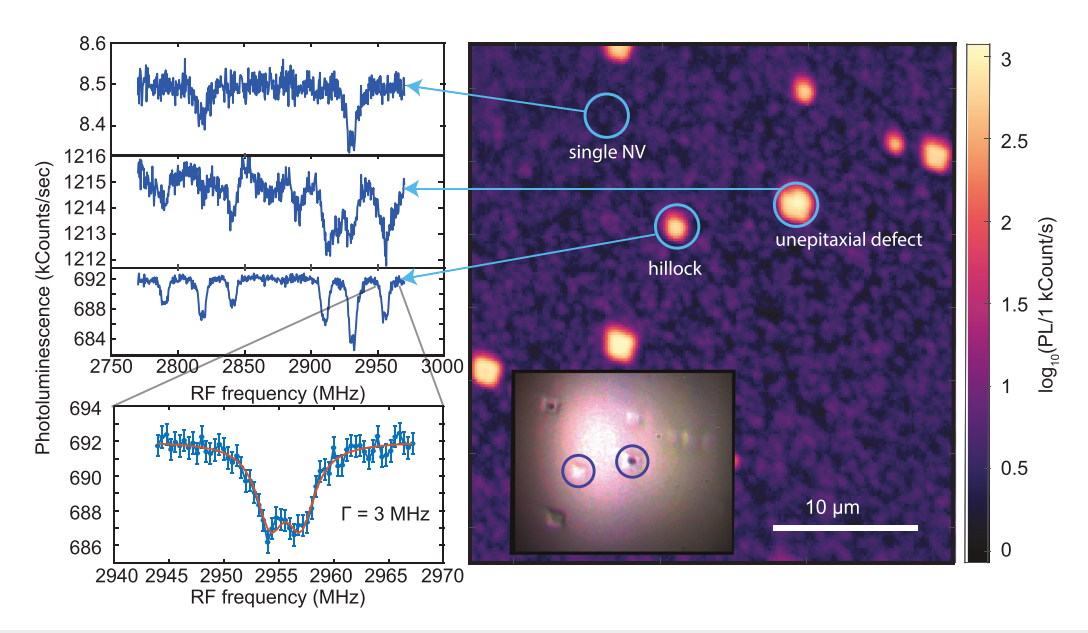


FIG. 5. Confocal photoluminescence image (right) of the $\theta=0.66^{\circ}$ miscut region showing a single NV center as well as NVs in a hillock and unepitaxial defect. Optically detected ESR spectra (left) illustrating similar linewidths of single NV centers and those within hillock defects. Spectra taken in the unepitaxial defect locations exhibit much broader linewidths.

larger linewidths and are likely strained or otherwise host an inhomogeneous material environment that results in the inhomogeneous broadening of NV centers. These results suggest that the hillock morphology may not compromise NV quality while offering a path toward significantly higher NV density; the measured hillock linewidths correspond to a $T_2^* \sim 300\,\mathrm{ns}$, which is consistent with the expected nitrogen-limited T^{2*36} for the estimated 10–20 ppm in the hillocks.

The initial miscut of the diamond seed substrate has been shown to be important for controlling a number of parameters in CVD growth for applications in quantum science. Namely, the growth rate, nitrogen density, and hillock density are all shown to depend on the miscut angle for growth conditions suited for quantum coherent applications, as reported here. Crucially, the mechanics of diamond growth change to a predominantly step bunching-dominated regime for $\theta \gtrsim 1.66^{\circ}$ and for sufficiently low angles transition to a regime of hillock-dominated growth. We conclude that an intermediate regime of optimal miscut exists around $\sim 1^{\circ}$ that is ideal for any application utilizing the doping techniques described. Finally, the enhanced incorporation of nitrogen at hillock defects is reported and, together with the narrow NV linewidths measured in the hillocks, invites further investigation of hillock-templated NV centers for, e.g., ensemble quantum sensing and incorporating many-body interacting spin systems into quantum applications. 37,38 Control over both lattice quality and nitrogen density is important for defect engineering in diamond, and miscut provides a powerful means for tuning both parameters.

See the supplementary material for further evidence to support our interpretation of the two nitrogen peaks present in the SIMS.

This work was supported as part of the Center for Novel Pathways to Quantum Coherence in Materials, an Energy Frontier Research Center funded by the U.S. Department of Energy, Office of Science, Basic Energy Sciences (defect characterization and materials growth) and by the U.S. Department of Energy, Office of Basic Energy Sciences, Division of Materials Sciences and Engineering under Award No. DE-SC0019241 (materials characterization). The MRL Shared Experimental Facilities are supported by the MRSEC Program of the NSF under Award No. DMR 1720256, a member of the NSF-funded Materials Research Facilities Network. S.A.M. acknowledges the support of the Natural Sciences and Engineering Research Council of Canada (NSERC) [Funding Reference No. AID 516704–2018] and the NSF Quantum Foundry through Q-AMASE-i program Award No. DMR-1906325.

DATA AVAILABILITY

The data that support the findings of this study are available from the corresponding author upon reasonable request.

REFERENCES

¹D. D. Awschalom, L. C. Bassett, A. S. Dzurak, E. L. Hu, and J. R. Petta, "Quantum spintronics: Engineering and manipulating atom-like spins in semi-conductors," Science 339, 1174–1179 (2013).

²M. Steger, K. Saeedi, M. L. W. Thewalt, J. J. L. Morton, H. Riemann, N. V. Abrosimov, P. Becker, and H.-J. Pohl, "Quantum information storage for over 180 s using donor spins in a ²⁸Si "semiconductor vacuum," Science 336, 1280–1283 (2012).

³D. D. Awschalom, R. Hanson, J. Wrachtrup, and B. B. Zhou, "Quantum technologies with optically interfaced solid-state spins," Nat. Photonics 12, 516–527 (2018).

⁴D. M. Toyli, D. J. Christle, A. Alkauskas, B. B. Buckley, C. G. Van de Walle, and D. D. Awschalom, "Measurement and control of single nitrogen-vacancy center spins above 600 k," Phys. Rev. X 2, 031001 (2012).

⁵G. Éthier-Majcher, D. Gangloff, R. Stockill, E. Clarke, M. Hugues, C. L. Gall, and M. Atatüre, "Improving a solid-state qubit through an engineered mesoscopic environment," Phys. Rev. Lett. 119, 130503 (2017).

- ⁶Y.-I. Sohn, S. Meesala, B. Pingault, H. A. Atikian, J. Holzgrafe, M. Gündoğan, C. Stavrakas, M. J. Stanley, A. Sipahigil, J. Choi et al., "Controlling the coherence of a diamond spin qubit through its strain environment," Nat. Commun. 9, 2012 (2018).
- ⁷B. A. Myers, A. Das, M. C. Dartiailh, K. Ohno, D. D. Awschalom, and A. C. Bleszynski Jayich, "Probing surface noise with depth-calibrated spins in diamond," Phys. Rev. Lett. 113, 027602 (2014).
- ⁸D. Bluvstein, Z. Zhang, and A. C. B. Jayich, "Identifying and mitigating charge instabilities in shallow diamond nitrogen-vacancy centers," Phys. Rev. Lett. 122, 076101 (2019).
- ⁹Y. Chu, N. de Leon, B. Shields, B. Hausmann, R. Evans, E. Togan, M. J. Burek, M. Markham, A. Stacey, A. Zibrov, A. Yacoby, D. Twitchen, M. Loncar, H. Park, P. Maletinsky, and M. Lukin, "Coherent optical transitions in implanted nitrogen vacancy centers," Nano Lett. 14, 1982–1986 (2014). pMID: 24588353
- 10 Y. Chu and M. D. Lukin, "Quantum optics with nitrogen-vacancy centers in diamond," arXiv:1504.05990 (2015).
- ¹¹D. Lee, K. W. Lee, J. V. Cady, P. Ovartchaiyapong, and A. C. B. Jayich, "Topical review: Spins and mechanics in diamond," J. Opt. 19, 033001 (2017).
- ¹²M. Mitchell, B. Khanaliloo, D. P. Lake, T. Masuda, J. P. Hadden, and P. E. Barclay, "Single-crystal diamond low-dissipation cavity optomechanics," Optica 3, 963–970 (2016).
- ¹³B. Khanaliloo, H. Jayakumar, A. C. Hryciw, D. P. Lake, H. Kaviani, and P. E. Barclay, "Single-crystal diamond nanobeam waveguide optomechanics," Phys. Rev. X 5, 041051 (2015).
- ¹⁴M. J. Burek, J. D. Cohen, S. M. Meenehan, N. El-Sawah, C. Chia, T. Ruelle, S. Meesala, J. Rochman, H. A. Atikian, M. Markham, D. J. Twitchen, M. D. Lukin, O. Painter, and M. Lončar, "Diamond optomechanical crystals," Optica 3, 1404–1411 (2016).
- ¹⁵J. V. Cady, O. Michel, K. W. Lee, R. N. Patel, C. J. Sarabalis, A. H. Safavi-Naeini, and A. C. B. Jayich, "Diamond optomechanical crystals with embedded nitrogen-vacancy centers," Quantum Sci. Technol. 4, 024009 (2019).
- ¹⁶T. Ishikawa, K.-M. C. Fu, C. Santori, V. M. Acosta, R. G. Beausoleil, H. Watanabe, S. Shikata, and K. M. Itoh, "Optical and spin coherence properties of nitrogen-vacancy centers placed in a 100 nm thick isotopically purified diamond layer," Nano Lett. 12, 2083–2087 (2012).
- ¹⁷K. Ohno, F. J. Heremans, L. C. Bassett, B. A. Myers, D. M. Toyli, A. C. Bleszynski Jayich, C. J. Palmstrøm, and D. D. Awschalom, "Engineering shallow spins in diamond with nitrogen delta-doping," Appl. Phys. Lett. 101, 082413 (2012).
- 18 J. Achard, V. Jacques, and A. Tallaire, "CVD diamond single crystals with NV centres: A review of material synthesis and technology for quantum sensing applications," J. Phys. D: Appl. Phys. 53(31), 313001 (2020).
- ¹⁹C. A. McLellan, B. A. Myers, S. Kraemer, K. Ohno, D. D. Awschalom, and A. C. Bleszynski Jayich, "Patterned formation of highly coherent nitrogen-vacancy centers using a focused electron irradiation technique," Nano Lett. 16, 2450–2454 (2016).
- 20 J. Butler, Y. Mankelevich, A. Cheesman, J. Ma, and M. Ashfold, "Understanding the chemical vapor deposition of diamond: Recent progress," J. Phys.: Condens. Matter 21, 364201–364220 (2009).

- ²¹N. Tokuda, M. Ogura, T. Matsumoto, S. Yamasaki, and T. Inokuma, "Influence of substrate misorientation on the surface morphology of homoepitaxial diamond (111) films," Phys. Status Solidi A 213, 2051–2055 (2016).
- ²²M. Lobaev, A. Gorbachev, S. Bogdanov, A. Vikharev, D. Radishev, V. Isaev, V. Chernov, and M. Drozdov, "Influence of cvd diamond growth conditions on nitrogen incorporation," Diamond Related Mater. 72, 1–6 (2017).
- ²³N. Tokuda, H. Umezawa, K. Yamabe, H. Okushi, and S. Yamasaki, "Hillock-free heavily boron-doped homoepitaxial diamond films on misoriented (001) substrates," Jpn. J. Appl. Phys., Part 1 46, 1469–1470 (2007).
- ²⁴M. Ogura, H. Kato, T. Makino, H. Okushi, and S. Yamasaki, "Misorientation-angle dependence of boron incorporation into (001)-oriented chemical-vapor-deposited (CVD) diamond," J. Cryst. Growth 317, 60–63 (2011).
- 25T. Yamamoto, S. D. Janssens, R. Ohtani, D. Takeuchi, and S. Koizumi, "Toward highly conductive n-type diamond: Incremental phosphorus-donor concentrations assisted by surface migration of admolecules," Appl. Phys. Lett. 109, 182102 (2016).
- ²⁶K. Hayashi, S. Yamanaka, H. Watanabe, T. Sekiguchi, H. Okushi, and K. Kajimura, "Diamond films epitaxially grown by step-flow mode," J. Cryst. Growth 183, 338–346 (1998).
- ²⁷A. Tallaire, M. Kasu, K. Ueda, and T. Makimoto, "Origin of growth defects in CVD diamond epitaxial films," <u>Diamond Related Mater.</u> 17, 60–65 (2008).
- ²⁸N. Tokuda, Homoepitaxial Diamond Growth by Plasma-Enhanced Chemical Vapor Deposition (Springer International Publishing, Cham, 2015), pp. 1–29.
- 29 Syntek, "Products-1: Various industrial diamonds," http://www.syntek.co.jp/en/products/.
- ³⁰See https://www.cameca.com/products/sims/ims7f-auto for "IMS 7f-Auto" (last accessed: March 24, 2020).
- ⁵³R. Wilson, "Sims quantification in Si, GaAS, and diamond—An update," Int. J. Mass Spectrom. Ion Processes 143, 43–49 (1995).
- 32T. R. Eichhorn, C. A. McLellan, and A. C. Bleszynski Jayich, "Optimizing the formation of depth-confined nitrogen vacancy center spin ensembles in diamond for quantum sensing," Phys. Rev. Mater. 3, 113802 (2019).
- 33 M. A. Lobaev, A. M. Gorbachev, S. A. Bogdanov, A. L. Vikharev, D. B. Radishev, V. A. Isaev, and M. N. Drozdov, "NV-center formation in single crystal diamond at different CVD growth conditions," Phys. Status Solidi A 215, 1800205 (2018).
- 34H. Okushi, H. Watanabe, S. Ri, S. Yamanaka, and D. Takeuchi, "Device-grade homoepitaxial diamond film growth," J. Cryst. Growth 237–239, 1269–1276 (2002).
- 35M. Shinohara and N. Inoue, "Behavior and mechanism of step bunching during metalorganic vapor phase epitaxy of GaAS," Appl. Phys. Lett. 66, 1936–1938 (1995).
- 36E. Bauch, S. Singh, J. Lee, C. A. Hart, J. M. Schloss, M. J. Turner, J. F. Barry, L. Pham, N. Bar-Gill, S. F. Yelin, and R. L. Walsworth, "Decoherence of dipolar spin ensembles in diamond," arXiv:1904.08763 (2019).
- 37H. Zhou, J. Choi, S. Choi, R. Landig, A. M. Douglas, J. Isoya, F. Jelezko, S. Onoda, H. Sumiya, P. Cappellaro, H. S. Knowles, H. Park, and M. D. Lukin, "Quantum metrology with strongly interacting spin systems," Phys. Rev. X 10, 031003 (2020)
- ³⁸S. Choi, N. Y. Yao, and M. D. Lukin, "Quantum metrology based on strongly correlated matter," arXiv:1801.00042 (2017).